# Experiments in DIII-D toward achieving rapid shutdown with runaway electron suppression[a)]

E. M. Hollmann,[1,b)] N. Commaux,[2] N. W. Eidietis,[3] T. E. Evans,[4] D. A. Humphreys,[4] A. N. James,[1] T. C. Jernigan,[2] P. B. Parks,[3] E. J. Strait,[4] J. C. Wesley,[3] J. H. Yu,[1] M. E. Austin,[4] L. R. Baylor,[2] N. H. Brooks,[3] V. A. Izzo,[1] G. L. Jackson,[3] M. A. van Zeeland,[3] and W. Wu[3]
[1]*University of California, San Diego, La Jolla, California 92093-0417, USA*
[2]*Oak Ridge National Laboratory, P.O. Box 2008, Oak Ridge, Tennessee 37831, USA*
[3]*General Atomics, P.O. Box 85608, San Diego, California 92186-5608, USA*
[4]*Fusion Research Center, University of Texas at Austin, Austin, Texas 78712, USA*

(Received 24 November 2009; accepted 11 January 2010; published online 6 May 2010)

Experiments have been performed in the DIII-D tokamak [J. L. Luxon, Nucl. Fusion **42**, 614 (2002)] toward understanding runaway electron formation and amplification during rapid discharge shutdown, as well as toward achieving complete collisional suppression of these runaway electrons via massive delivery of impurities. Runaway acceleration and amplification appear to be well explained using the zero-dimensional (0D) current quench toroidal electric field. 0D or even one-dimensional modeling using a Dreicer seed term, however, appears to be too small to explain the initial runaway seed formation. Up to 15% of the line-average electron density required for complete runaway suppression has been achieved in the middle of the current quench using optimized massive gas injection with multiple small gas valves firing simultaneously. The novel rapid shutdown techniques of massive shattered pellet injection and shell pellet injection have been demonstrated for the first time. Experiments using external magnetic perturbations to deconfine runaways have shown promising preliminary results. © *2010 American Institute of Physics*.
[doi:10.1063/1.3309426]

## I. INTRODUCTION

Avoiding wall damage due to disruptions is expected to be an important issue in future reactor-size tokamaks.[1,2] Ideally, disruptions will be largely prevented altogether by real-time recognition of stability barriers and avoiding control system failures. In the rare event of an unavoidable disruption, however, it will be important to implement a rapid shutdown system which can safely and rapidly terminate the discharge while minimizing wall damage due to the plasma thermal and magnetic energy. Presently, massive gas injection (MGI) is envisioned as the rapid shutdown method for ITER and has been tested successfully in a variety of present-day tokamaks.[3–7] Conducted heat loads to the divertor and halo current forces in the vessel walls are observed to be small when compared with major unmitigated disruptions, especially beta-limit disruptions and hot vertical displacement (VDE) disruptions.[8] Also, generation of runaway electrons (REs) is typically found to be very small during MGI shutdowns. It is generally thought that the heat load and halo current reduction capabilities of MGI shutdown will scale well to ITER; however, RE formation is a concern because of the additional RE seed terms (Compton scattering and tritium beta decay) and larger RE amplification (knock-on avalanche) in ITER when compared with present devices.[9]

Because of their importance for ITER, study of REs produced during discharge startup, during disruptions, and during rapid shutdowns is an active area of research in the tokamak community. Evidence for RE amplification (avalanching) has been seen in startup REs,[10] disruption REs,[11] and rapid shutdown REs.[12] Estimates of disruption RE seed terms have been made and, in some cases, might be consistent with the standard Dreicer RE growth rate.[12] Disruptions with strong RE formation showed the formation of very stable, long-lived (hundreds of milliseconds) RE beams.[13] The RE beams have been imaged during MGI experiments with IR synchrotron emission,[12] during startup with visible emission,[14] and during disruptions with soft x-ray (SXR) tomography.[11] Overall, the REs tend to form a circular ($D \sim 10-40$ cm) beam which tends to drift vertically during the current quench (CQ).[11] Typically, energies near the synchrotron limit ($\varepsilon \sim 50$ MeV) are observed.[15] Experiments were performed to try to deconfine REs with externally applied magnetic field errors. Evidence for enhanced RE loss from external magnetic perturbations was seen on startup REs,[16] disruption REs,[17] and on rapid shutdown REs.[18]

In DIII-D, recent disruption work focused on developing a massive-delivery rapid shutdown system which can deliver sufficient mass to the plasma current channel to achieve total collisional suppression of RE formation. These experiments focused on three approaches: MGI, shattered cryogenic pellets, and shell pellets. DIII-D MGI experiments found that impurity assimilation is optimized by firing many small valves simultaneously in a short (~2 ms pulse), as opposed to firing a single large valve. Large shattered cryogenic pellet

[a)]Paper XI3 4, Bull. Am. Phys. Soc. **54**, 345 (2009).
[b)]Invited speaker. Electronic mail: ehollmann@ucsd.edu.

 

shutdowns were performed using $D \sim 1.3$ cm frozen $D_2$ pellets shattered by a breaker plate. These first experiments achieved extremely high local electron densities $n_e \approx 7 \times 10^{15}$ cm$^{-3}$ in the injection region during the thermal quench (TQ), although line-average electron densities achieved in the middle of the CQ were comparable to those achieved by $D_2$ MGI, $n_e \approx 2 \times 10^{15}$ cm$^{-3}$. Proof-of-principle shell pellet experiments were performed using small $D = 2$ mm hollow polystyrene shells to successfully deliver dispersive payloads (Ar gas or boron powder) to the plasma core. Larger shell pellet experiments firing $D = 1$ cm hollow polystyrene shells through discharges were attempted; however, these larger shell pellets did not break open, so payload release was not achieved.

In addition to these high-mass rapid shutdown experiments, experiments have been pursued toward understanding the physics of RE production, transport, and amplification during rapid shutdowns. These experiments typically use small cryogenic argon pellet injection to create a rapid shutdown with a significant RE population. Evidence for RE avalanching has been seen, with a growth rate $\tau \approx 2$ ms, consistent with theory. RE energies of order of 30–40 MeV have been measured, consistent with simple zero-dimensional (0D) models. The RE seed formation in these experiments is not well understood at present: the seed amplitude appears to vary by several orders of magnitude in similar shots and can be much larger than expected from simple 0D Dreicer models.

This paper is organized as follows: Section II gives a description of the experimental setup, Sec. III describes experiments on rapid shutdown REs, Sec. IV describes massive-delivery rapid shutdown experiments, Sec. V describes experiments to deconfine REs with external magnetic fields, and Sec. VI contains a brief discussion and conclusions.

## II. EXPERIMENTAL SETUP

The experiments described here are typically performed with lower single null H-mode discharges in the DIII-D tokamak.[19] About 2–6 MW of heating is supplied from one to three neutral beam sources. Typical initial (preshutdown) experimental parameters are toroidal magnetic field $B_\varphi = 2.1$ T, toroidal plasma current $I_p = 1.5$ MA, central electron temperature $T_{e,0} = 2.5$ keV, and central electron density $n_{e,0} = 8 \times 10^{13}$ cm$^{-3}$.

Figure 1(a) shows a top view of the tokamak and some of the hardware used in these experiments. Rapid shutdown is initiated by either MGI, shattered pellet injection, small cryogenic pellet injection, or shell pellet injection; these methods typically have vacuum trajectories aimed roughly at the plasma magnetic axis. Injected impurities are (except for the small cryogenic pellets) viewed directly by a fast-framing visible camera. SXR/bolometer arrays close to the injection region can be used to obtain fast radiated power or SXR data. Extreme/vacuum ultraviolet (EUV/VUV) survey spectra are obtained with a fast single-chord UV spectrometer. The main electron density measurement is a four-chord $CO_2$ interferometer. The main RE diagnostic is a hard x-ray

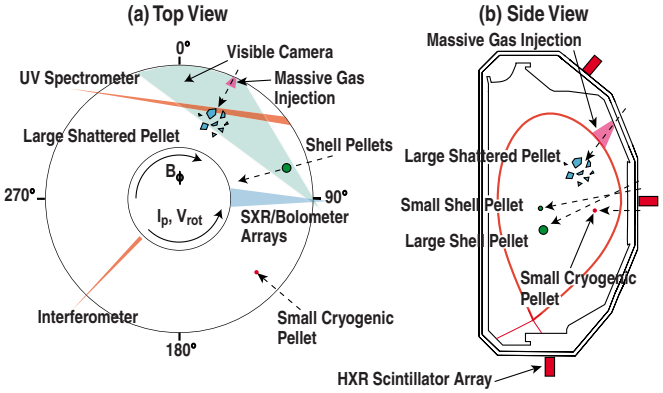


FIG. 1. (Color online) (a) Top view of tokamak showing locations of diagnostics and (b) poloidal cross section of initial plasma magnetic flux surfaces and gas jet location.

(HXR)/gamma scintillator array consisting of 12 barium germanium oxide (BGO) scintillators placed around the machine outside the vacuum vessel at six toroidal locations and three poloidal locations. At two locations, multiple colocated BGO scintillators with varying lead thickness are used to provide HXR energy information. A single high-gain photomultiplier tube (PMT)-coupled plastic scintillator (not shown in Fig. 1) is used to estimate RE currents in cases where the BGO scintillator signal levels are too low. Both BGO and plastic scintillators measure HXRs with energies $\varepsilon > 0.5$ MeV which are created when REs strike the vessel wall.

## III. RAPID SHUTDOWN RUNAWAY ELECTRON EXPERIMENTS

Figure 2 gives an overview of RE currents generated during various types of rapid shutdowns in DIII-D. Shots above the upper dashed line are "large RE shots," where the RE current $I_{RE}$ can be estimated by fitting the observed plasma current trace to separate Ohmic (exponentially decaying) and runaway (the remainder) components. For shots be-

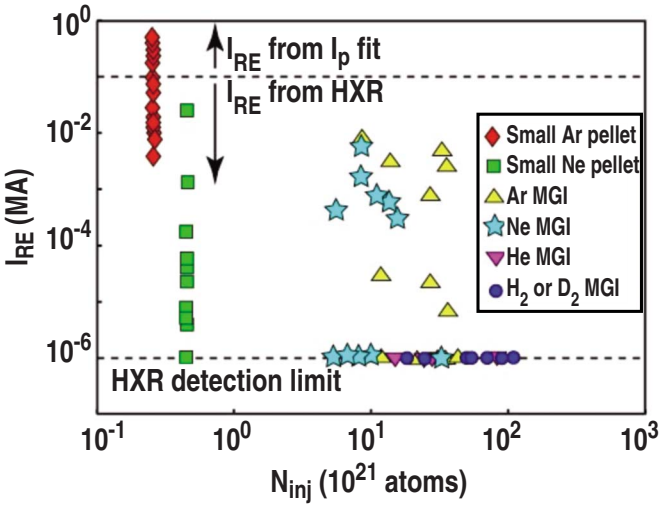


FIG. 2. (Color online) RE current $I_{RE}$ during rapid shutdown experiments as a function of $N_{inj}$ the number of atoms injected.

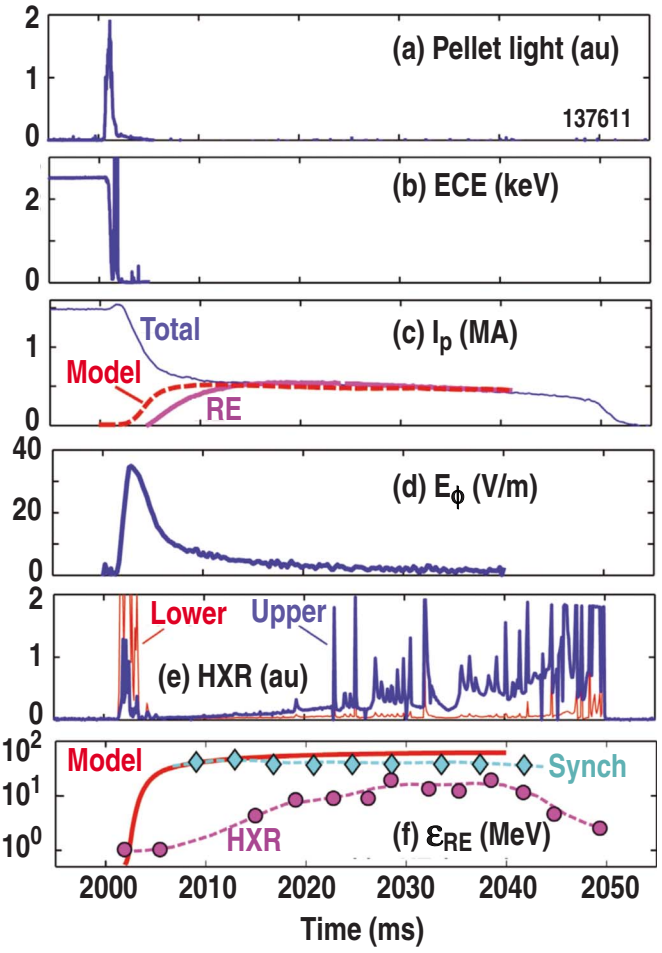


FIG. 3. (Color online) Time traces of a small Ar pellet shutdown showing (a) pellet light, (b) ECE, (c) plasma current, (d) 0D electric field, (e) upper (thick curve) and lower (thin curve) HXR scintillations, and (f) measured (points) and modeled (solid curve) RE energy.

low this upper dashed line ("small RE shots"), $I_{RE}$ is estimated from the integrated intensity of the BGO or (for very weak RE cases) plastic scintillator flash seen at the end of the CQ (with an approximate cross calibration obtained from large RE shots). Points lying on the lower dashed line are in the noise level of the plastic scintillator, so only a rough upper bound (perhaps 1 A) can be placed on $I_{RE}$. Overall, it can be seen that the largest RE currents are created by small Ar pellet injection, so this technique is most typically used for RE studies in DIII-D. The scatter in RE production shot-shot can be seen to be quite large: for nominally similar initial conditions, for example, neon pellet injection appears to generate more than four orders of magnitude variation in RE current. Massive injection of low-$Z$ materials (He, $H_2$, or $D_2$) typically does not generate measurable REs; this is also the case for natural disruptions in DIII-D.

Figure 3 gives an overview of time traces from a large RE shot, where a small Ar pellet is fired into the tokamak. The pellet hits the plasma at $t \approx 2000$ ms, as seen by the pellet visible light emission, Fig. 3(a). The pellet quickly causes the plasma TQ, shown by the sudden drop in electron cyclotron emission (ECE) Fig. 3(b). The nonthermal ECE spike seen in Fig. 3(b) immediately after the TQ drop is believed to be due to confined (on axis) REs with energies of order of 0.1–2 MeV; this suggests a very prompt (during the TQ) formation of REs.

Figure 3(c) shows the total measured plasma current $I_p$ (thin curve) as well as the estimated RE current (thick curve) obtained by subtracting off an exponential fit to the initial current decay. The dashed curve in Fig. 3(c) is the result of an avalanche model in which the RE seed term is varied and allowed to amplify due to the 0D electric field $E_\phi$ according to the standard knock-on avalanche growth rate.[20] It can be seen that the predicted avalanche growth rate of about 2 ms is consistent with the measured runaway current growth rate. To obtain the good fit shown here, a seed term of 8 kA was used, suggesting an avalanche gain of about 50 in this shot.

Figure 3(d) shows the average (0D) toroidal electric field $E_\phi$ estimated from magnetic pickup loops. This is done by using magnetic loop signals to calculate an approximate plasma current density distribution. Changes in this current density can then be used to estimate an average (0D) toroidal electric field $E_\phi$ experienced by the plasma using a simple circuit equation which includes the plasma self-inductance as well as mutual inductances between the plasma current and fixed external conductors (wall and coils). Figure 3(e) shows raw data from two BGO scintillators—an upper scintillator (thick curve) mounted above the machine and a lower scintillator (thin curve) mounted below the machine. It can be seen that there is an early loss of REs at the end of the TQ ($t \approx 2000$ ms) which is stronger in the bottom of the machine; this "prompt loss" flash is thought to be REs which are born on stochastic field lines and are thus lost rapidly, as predicted by NIMROD modeling.[21] REs born near the magnetic axis on good flux surfaces are better confined, but scrape off against the wall as the RE current channel drifts up, giving a larger signal on the upper HXR detector later in the shot $t \approx 2020-2050$ ms. This upward drift of the RE beam is seen consistently in strong RE shots but is not fully understood at present, although control system forces (as opposed to inherent drifts) are suspected to be responsible. Figure 3(f) shows RE energy $\varepsilon_{RE}$ as a function of time. The diamonds are $\varepsilon_{RE}$ estimated from visible synchrotron brightness, while the circles are a lower bound on $\varepsilon_{RE}$ obtained from HXR intensities measured at the outer midplane. The solid curve is $\varepsilon_{RE}$ estimated from a simple 0D model which assumes that REs gain energy from the toroidal field $E_\phi$ and lose energy due to synchrotron radiation. It can be seen that the model and the data are reasonably consistent, within 50%.

## IV. MASSIVE-DELIVERY RAPID SHUTDOWN EXPERIMENTS

As shown in Fig. 2, massive injection of low-$Z$ gas into DIII-D does not generate any measurable RE current. However, the long CQ time (~50 ms) and corresponding large RE avalanche gain $G > 10^{10}$ predicted for ITER means that even tiny RE seeds $I_{RE} < 1$ A not detectable here could amplify to dangerous (megampere) levels.[20] Because of this, experiments in DIII-D are investigating the feasibility of delivering sufficient mass into the current channel to com-

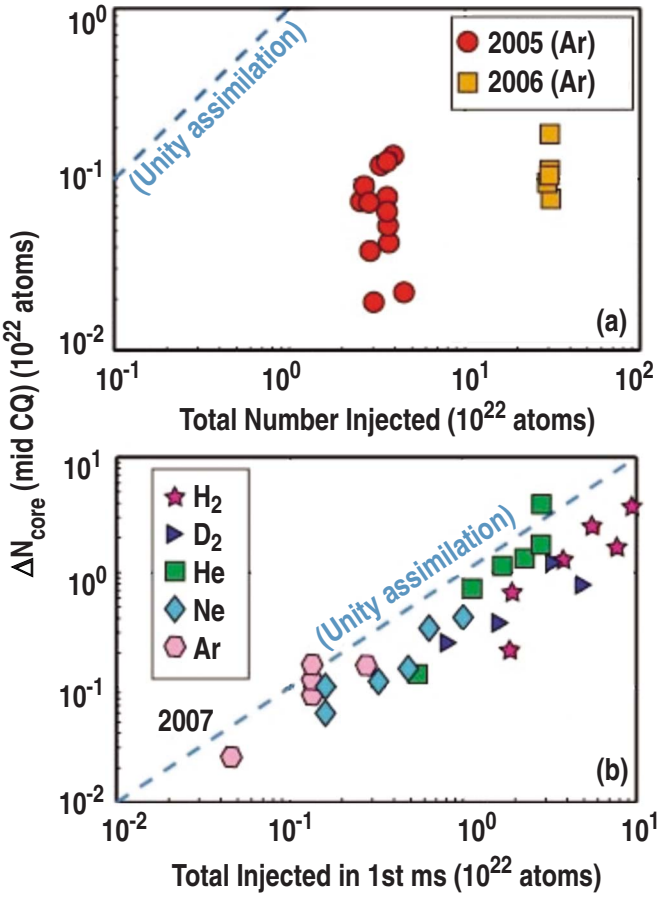


FIG. 4. (Color online) Number of atoms assimilated into the plasma core by the middle of the CQ, $N_{core}$, as a function of (a) the total number of atoms injected and (b) the amount injected in the first millisecond for MGI experiments.

pletely suppress any RE production; this is predicted to occur at very high total electron densities $n_{tot}=n_e+0.5n_{bound}>n_{crit}$, where $n_{crit}\approx 8\times 10^{14}\ \mathrm{cm}^{-3}\times E_\phi$, with $E_\phi$ in (V/m).[20] Due to the rapid TQ onset and loss of stored thermal energy when impurities are introduced into the plasma edge, delivering and maintaining this large density in the current channel during the CQ is extremely challenging. Three different massive-delivery methods are being investigated: MGI, shattered pellet injection, and shell pellet injection.

### A. Massive gas injection

Progress has been made at improving ion assimilation with MGI in DIII-D mainly by using faster gas delivery to the plasma edge. Using multiple (up to six) small MGI valves firing simultaneously was found to give a cleaner, faster-rising gas pulse than using a single large valve. Any obstructions in the gas delivery drift tube were found to adversely affect assimilation efficiency.

Figure 4 illustrates the improvement in DIII-D MGI assimilation efficiency over the last few years. In Fig. 4(a), 2005 data used a small ($D=0.4$ cm) fast valve to deliver of order of 1000 Torr-liter of argon to the plasma in a pulse of order of 15 ms long. 2006 data used a single large ($D=2$ cm) fast valve to deliver of order of 10 000 Torr-liter of argon to the plasma in a pulse of order of 10 ms long. Plotting the total amount of atoms injected versus the amount assimilated into the plasma in the middle of the CQ, $\Delta N_{core}\equiv\Delta\bar{n}_e V_p/\langle Z\rangle(t=t_{mid,CQ})$, shows a very low (of order of 1% or worse) overall assimilation efficiency. The increase in line-average electron density $\bar{n}_e$ is estimated from a central interferometer view chord and the mean charge state $\langle Z\rangle$ is estimated by assuming ionization/recombination equilibrium at the measured CQ electron temperature $T_e$. The average electron temperature during the CQ is measured by a combination of techniques—UV carbon line ratios, He free-bound continuum slope, and Langmuir probe sweeps.[22]

Figure 4(b) shows 2007 MGI data which used a variable number (1–6) of small ($D=0.4$ cm) fast valves fired simultaneously in a short (~1–2 ms) long pulse. The amount assimilated $\Delta N_{core}$ is plotted as a function of the number of atoms injected in the first millisecond, demonstrating relatively good assimilation of particles delivered in the first 1 ms. Overall, we find that MGI impurity assimilation can be predicted reasonably well by assuming that gas injected before or during the TQ is assimilated with 10%–20% efficiency and gas arriving after this (during the CQ) is not assimilated.

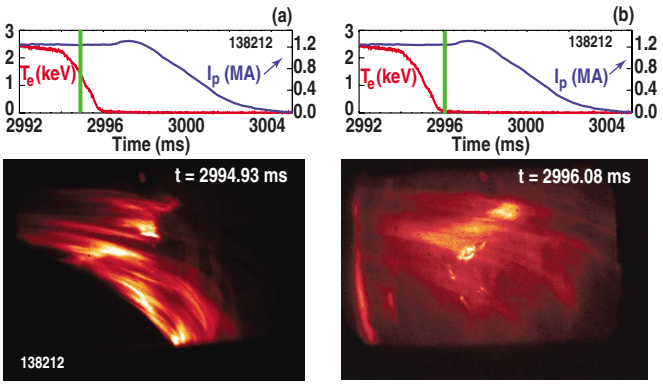


FIG. 5. (Color online) Unfiltered visible light images of a $D_2$ shattered pellet fast shutdown taken (a) in the middle of the TQ and (b) at the end of the TQ.

### B. Shattered pellet injection

Experiments were begun in 2009 to investigate rapid shutdown with large shattered pellets.[23] In these experiments, a single large ($D\sim 1.3$ cm) frozen deuterium pellet is fired into the vacuum chamber. At the first wall, the pellet is shattered by a v-groove which directs the resulting mixture of deuterium ice shards and liquid toward the plasma core. The ice shards are observed by camera imaging and fast bolometry to penetrate into the plasma core rapidly, resulting in a very rapid (~1 ms duration) TQ (as compared with ~2 ms more typical for deuterium MGI). An example of fast camera images taken during shattered pellet experiments is shown in Fig. 5. Figure 5(a) shows a mid-TQ image and Fig. 5(b) shows an image at the end of the TQ. Unfiltered light images are shown here. Localized bright spots believed to be ice shards of $D_2$ can be seen traversing the plasma cross section in the images [see Fig. 1(a) for the camera field of view]. Very high toroidally localized electron densities up to $n_e$

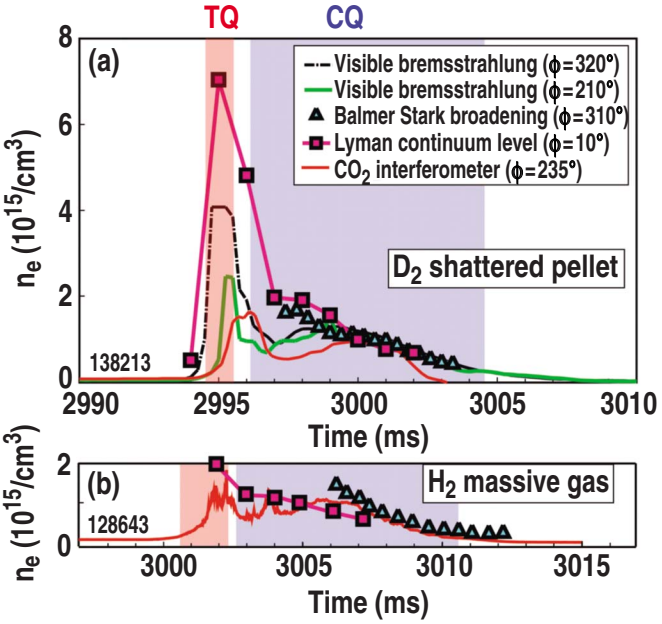


FIG. 6. (Color online) (a) Electron density $n_e$ measured at various toroidal locations following (a) massive shattered $D_2$ pellet injection and (b) massive $H_2$ gas injection.

$\approx 7\times 10^{15}$ cm$^{-3}$ are observed near the injection location $\phi = 0.5°$ during the TQ. Various electron density diagnostics then show this density perturbation rapidly equilibrating toroidally, Fig. 6(a). By the middle of the CQ, lower values are measured, similar to $D_2$ or $H_2$ MGI, Fig. 6(b). The present shattered pellet experiments are far from optimized—microwave cavity signals indicate that the initial (preshattering) ice pellets break off in two or more pieces, with a significant fraction of the resulting ice shards arriving after the TQ is over. Future experiments will attempt to form a single ice pellet, rather than several, in the launch tube. Shutdown with higher-$Z$ (e.g., neon) shattered pellets will also be studied.

### C. Shell pellet injection

The third massive-injection rapid shutdown scheme being investigated at DIII-D is shell pellet injection. The basic idea is to fire a pellet consisting of a hard shell and dispersive payload at the plasma. The hard shell ablates away as the pellet transits through the plasma edge. Upon reaching the plasma core, the shell breaks open, releasing the dispersive payload throughout the core region. Two different types of dispersive payloads have been proposed: dust grains[24] or high-pressure gas.[25]

Proof-of-principle shell pellet experiments were conducted in DIII-D using small (o.d. $\approx 2$ mm, $t \approx 0.4$ mm) polystyrene shells filled with either pressurized (10 atm) argon gas or with boron powder.[26] The pellets were fired at an initial velocity $v = 350$ m/s at the plasma core. These small shell pellets did not disrupt the plasma, but penetrated in to normalized minor radius $r/a \approx 0.5$ before burning through and releasing their payload. The payload release, ionization, and rapid (within about 10 ms) dispersion through the core was observed in visible camera imaging, with charge-exchange recombination and with UV spectroscopy. Figure 7 shows UV spectrometer data showing flashes of highly stripped argon and boron line emission from (a) an argon-filled pellet and (b) a boron-filled pellet.

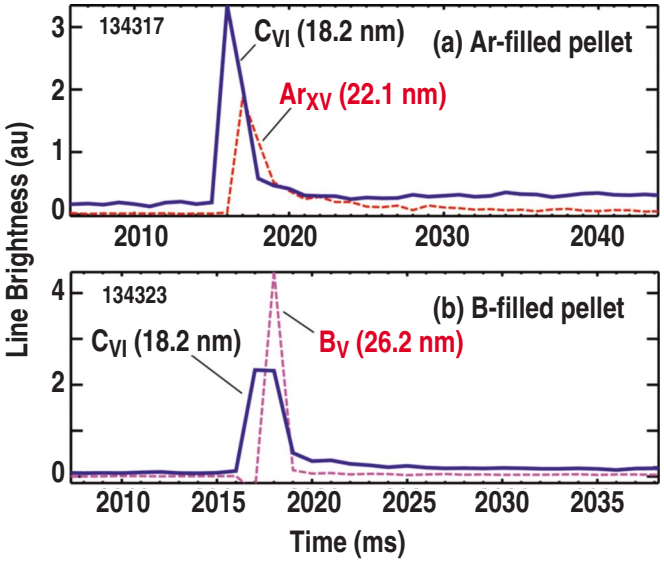


FIG. 7. (Color online) UV line brightness vs time for small shell pellets filled with (a) argon gas and (b) boron powder.

Following the successful demonstration of the shell pellet concept with small shell pellets, large shell pellet experiments were attempted in 2009. In these experiments, large (o.d. $\approx 1$ cm, $t \approx 0.4$ mm) polystyrene shells filled with boron powder were fired at velocity $v \approx 200$ m/s through the plasma core. These large shell pellets did shut down the discharge and initiate the TQ but did not break open in the plasma. Figures 8 and 9 compare pellet radial trajectories and shell wall burn through for a small shell pellet and a large shell pellet. Pellet trajectory and burn through are both estimated from fast camera data—the trajectory by assuming the out-of-plane position is close to the vacuum trajectory

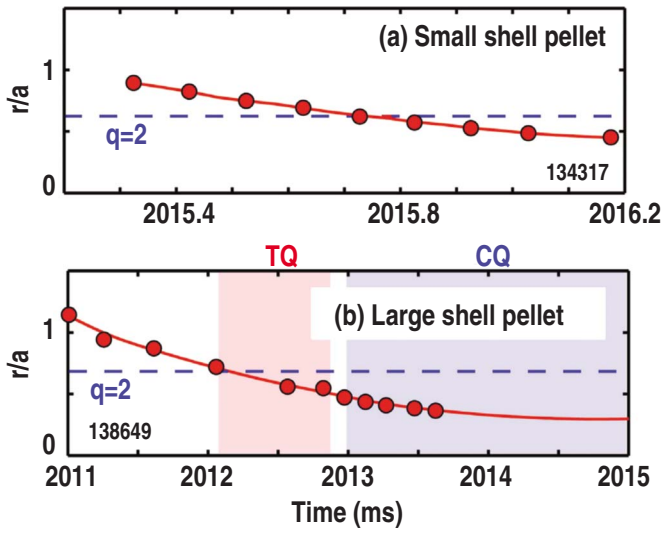


FIG. 8. (Color online) Pellet trajectories $r/a$ as a function of time for (a) a small shell pellet and (b) a large shell pellet.

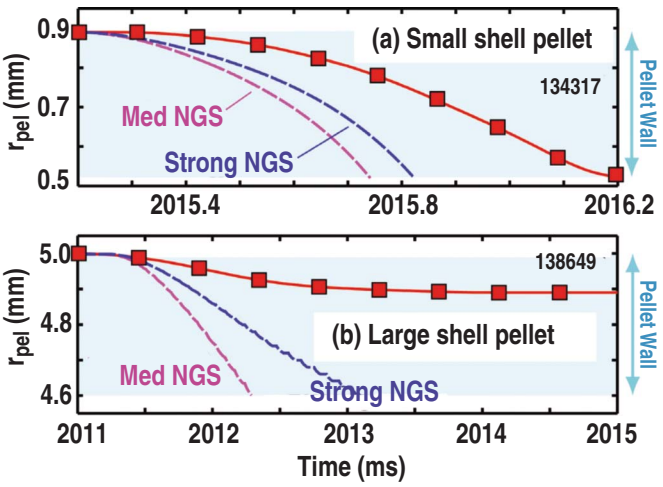


FIG. 9. (Color online) Pellet burn through as a function of time for (a) a small shell pellet and (b) a large shell pellet. The solid curves show measurements and dashed curves show ablation models.

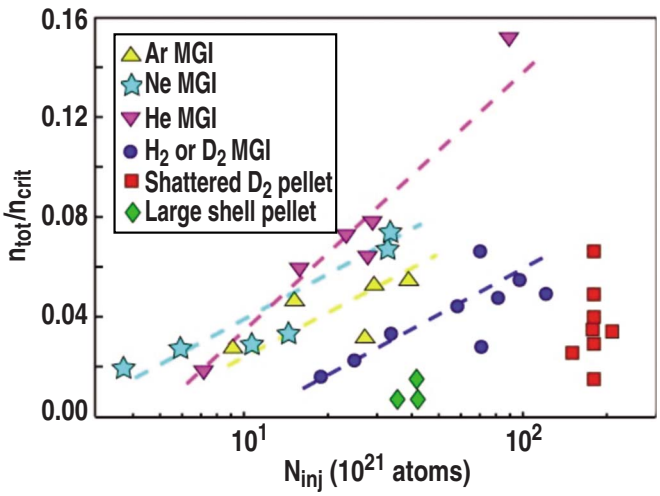


FIG. 10. (Color online) Collisional RE suppression density $n_{tot}/n_{crit}$ during rapid shutdown experiments as a function of $N_{inj}$ the number of atoms injected.

(confirmed by center stack strike marks in the case of the large shell pellets); and the burn through by assuming that pellet ablation rate is proportional to ablation plume brightness, with a normalization of mass ablated obtained using total observed electron density rise from interferometers. Figure 8(a) shows the small shell pellet trajectory—the pellet can be seen to reach about half way into the core $r/a \approx 0.5$ before burning up. Figure 8(b) shows the large shell pellet trajectory—the pellet can be seen to initiate the TQ upon crossing the $q=2$ surface. The curve in Fig. 8(b) is due to the pellet trajectory missing the plasma magnetic axis.

Solid curves in Fig. 9 show burn through of the pellet walls as a function of time for (a) a small shell pellet and (b) a large shell pellet. From Fig. 9(b), it is apparent that the large shell pellet wall is estimated to have ablated about one-fourth of the way through. After $t \approx 2013$ ms (end of the TQ), ablation effectively turns off and the large shell pellet passes through the rest of the plasma unperturbed. These data suggest that the pellet walls need to be made about 100 $\mu$m thick for large shell pellets to work in DIII-D. The dashed curves give estimates of the polystyrene shell ablation predicted from ablation models. The models shown here are "med-NGS"—a neutral gas shielding ablation model which does not include electrostatic shielding[27] and "strong NGS" a similar model including electrostatic shielding.[28] Overall, the models do a reasonably good job of predicting the small shell pellet ablation, but are somewhat optimistic at predicting large shell pellet ablation—this discrepancy could arise from precooling (anomalous heat transport at the strongly perturbing large pellet cold front).

### D. Overview of massive-delivery experiments

Figure 10 plots the normalized collisional RE suppression density $n_{tot}/n_{crit}$ achieved during rapid shutdown experiments as a function of $N_{inj}$, the total number of atoms injected. The ratio $n_{tot}/n_{crit}$ is evaluated in the middle of the CQ, with the electric field $E_\phi$ estimated in a 0D approximation from the measured plasma current decay rate. Only optimized "short pulse" multivalve MGI data are shown, with increased $N_{inj}$ achieved for each species by increasing the number of MGI valves fired simultaneously. Overall, it can be seen that greater values of $n_{tot}/n_{crit}$ are achieved by injecting more gas, with a highest value $n_{tot}/n_{crit} \approx 0.15$ achieved using five valve helium MGI. Presently, the shattered pellet experiments (squares in Fig. 10) do not appear to give better 0D mid-CQ $n_{tot}/n_{crit}$ than comparable MGI ($D_2$ or $H_2$). The $n_{tot}/n_{crit}$ for the large shell pellets (diamonds) can be seen to be quite low; however, we anticipate that a large improvement can be achieved once the shell is made thin enough to allow the dispersive payload to be released. Also, we anticipate that improvements can be made in MGI performance (with more valves mounted closer to the plasma) and in shattered pellet performance (with a single pulse of shards rather than several).

## V. RUNAWAY ELECTRON DECONFINEMENT USING EXTERNAL MAGNETIC PERTURBATIONS

Because of the high electron velocity, electron confinement is known to be especially sensitive to magnetic field errors. Using external magnetic field perturbations to deconfine RE seeds, sending them into the wall before they have time to avalanche and accelerate to high energies during the CQ, was proposed previously[29] and promising preliminary results were obtained in various tokamaks.[17,18] Magnetohydrodynamic (MHD) simulations have been performed on this effect and indicate that RE confinement can be destroyed by relatively small stochastic field amplitudes $\delta B/B \approx 10^{-3}$.[30,31] However, simulations also indicate that maintaining a stochastic region across the entire plasma profile throughout the CQ might be challenging due to flux surface healing.[21]

Experiments have been performed on DIII-D to study the deconfinement of RE seeds by applying nonaxisymmetric magnetic fields. Promising results have been obtained for weak RE seed shots with an applied $n=3$ perturbation (where $n$ is the toroidal mode number). Figure 11 shows a sequence

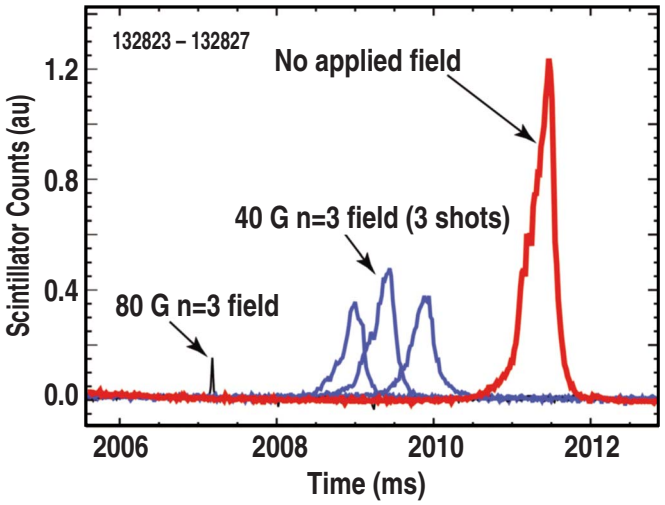


FIG. 11. (Color online) Plastic gamma scintillator counts as a function of time for different amplitudes of applied $n=3$ magnetic fields showing reduction in amplitude of RE current hitting wall.

of five repeat shots where a weak RE seed is created with single valve neon MGI and various amplitudes of $n=3$ perturbations applied. The $n=3$ field perturbation in these experiments is turned on long (0.5 s) before the shutdown. The field strengths shown in Fig. 11 are the radial vacuum magnetic field $n=3$ amplitude at the outer separatrix midplane; the applied fields thus correspond to fairly large relative perturbations $\delta B_r/B_\phi \approx 4\times 10^{-3}$. The poloidal $(m)$ spectrum of the applied perturbation is broad, covering $m\approx 1-15$ as the coils are localized near the outer midplane. For the target plasmas used here, the strongest resonance in the plasma is thought to be around $m\approx 12$. Plastic scintillator counts as a function of time are shown (as discussed above, this is believed to provide a reasonable estimate of RE current hitting the wall). A clear trend of decreasing RE current with increased $n=3$ field can be seen, suggesting that REs are being deconfined and lost to the wall earlier as a result of the applied field. Similar experiments using $n=1$ did not show as a clear trend, nor did experiments on shots with large RE currents. However, the large RE seed term variability makes these experiments challenging to interpret, so future experiments are planned to add more data points to help interpret this effect.

## VI. DISCUSSION AND CONCLUSIONS

In summary, a variety of experiments have been performed on the DIII-D tokamak to study formation and amplification of REs during fast shutdowns. RE amplification during the CQ is found to be consistent with avalanche theory using 0D electric fields, giving a growth time of order of 2 ms and total amplification during the CQ of order of 50. RE acceleration up to of order of 30–40 MeV is measured, also consistent with expected 0D electric fields. A large scatter of several orders of magnitude is observed in the final RE current; presently, this scatter is suspected to be a result dominantly of large scatter in the initial RE seed. RE seed currents of order of 10 kA are estimated for large RE shots. These seeds appear too large to be explained with preliminary estimates using the 0D electric field and the Dreicer RE seed model,[32] which gives an approximate RE seed $I_{RE}\approx 10^{-20}$ A for our experiments. Preliminary efforts have been made to model the large RE shots with a one-dimensional current diffusion model; in this case a significantly larger Dreicer seed $I_{RE}\approx 10$ A is estimated; however, this is still three orders of magnitude smaller than the experiment. This contrasts with MGI experiments on TEXTOR, where it was concluded that the measured REs could be explained by a 0D Dreicer seed plus a small approximately five-fold avalanche amplification.[12] Because of the exponential dependence of the Dreicer seed on plasma parameters and the difficulty of accurately measuring plasma parameters during the TQ, it is possible that this discrepancy arises from measurements uncertainties. It is also possible that the RE seeds in these experiments come from very localized electric fields requiring a two-dimensional or even three-dimensional model; from time-dependent effects such as hot-tail formation[31,33] or from magnetic reconnection during the TQ MHD.[34]

Experiments are being performed to investigate the feasibility of collisionally suppressing REs with massive impurity injection. Massive gas injection has been optimized by using multiple small valves firing simultaneously. This method has enabled achievement of 15% of the critical density with He MGI. First-of-a-kind experiments on rapid shutdown using large shattered deuterium pellets have been performed. These experiments resulted in record localized electron densities during the TQ in DIII-D. Also, first-of-a-kind experiments on rapid shutdown using shell pellets have been performed. The small shell pellets successfully demonstrated the shell pellet principle, depositing dispersive payloads into the plasma core. The large shell pellets were made too thick and did not release their payload, demonstrating the need for thinner-than-expected pellet walls when using large shell pellets.

Finally, first DIII-D experiments on deconfining rapid shutdown REs using external magnetic perturbations have been performed. Preliminary, encouraging results have been obtained with an $n=3$ perturbation acting on a small RE current generated by neon MGI.

## ACKNOWLEDGMENTS

The technical assistance of the DIII-D staff, especially B. Williams with the large shell pellet injector, D. Sundstrom with the small shell pellet injector, and J. Kulchar with diagnostics, is gratefully acknowledged. This work supported in part by the U.S. Department of Energy under Contract Nos. DE-FG02-07ER54917, DE-FG02-05ER54809, DE-AC05-00OR22725, DE-FC02-04ER54698, DE-FG02-95ER54309, and DE-FG03-97ER54415.

[1] F. C. Schuller, Plasma Phys. Controlled Fusion **37**, A135 (1995).
[2] ITPA MHD, Disruption and Magnetic Control Topical Group, T. C. Hender, J. C. Wesley, J. Bialek, A. Bondeson, A. H. Boozer, R. J. Buttery, A. Garofalo, T. P. Goodman, R. S. Granetz, Y. Gribov, O. Gruber, M. Gryaznevich, G. Giruzzi, S. Günter, N. Hayashi, P. Helander, C. C. Hegna, D. F. Howell, D. A. Humphreys, G. T. A. Huysmans, A. W. Hyatt, A. Isayama, S. C. Jardin, Y. Kawano, A. Kellman, C. Kessel, H. R. Koslowski, R. J. La Haye, E. Lazzaro, Y. Q. Liu, V. Lukash, J. Manickam, S.

Medvedev, V. Mertens, S. V. Mirnov, Y. Nakamura, G. Navratil, M. Okabayashi, T. Ozeki, R. Paccagnella, G. Pautasso, F. Porcelli, V. D. Pustovitov, V. Riccardo, M. Sato, O. Sauter, M. J. Schaffer, M. Shimada, P. Sonato, E. J. Strait, M. Sugihara, M. Takechi, A. D. Turnbull, E. Westerhof, D. G. Whyte, R. Yoshino, and H. Zohm, Nucl. Fusion **47**, S128 (2007).
[3]V. Riccardo, P. Andrew, L. C. Ingesson, and G. Maddaluno, Plasma Phys. Controlled Fusion **44**, 919 (2002).
[4]M. Bakhtiari, Y. Kawano, H. Tamai, Y. Miura, R. Yoshino, and Y. Nishida, Nucl. Fusion **42**, 1197 (2002).
[5]D. G. Whyte, T. C. Jernigan, D. A. Humphreys, A. W. Hyatt, C. J. Lasnier, P. B. Parks, T. E. Evans, P. L. Taylor, A. G. Kellman, D. S. Gray, and E. M. Hollmann, J. Nucl. Mater. **313–316**, 1239 (2003).
[6]R. S. Granetz, E. M. Hollmann, D. G. Whyte, V. A. Izzo, G. Y. Antar, A. Bader, M. Bakhtiari, T. Biewer, J. A. Boedo, T. E. Evans, I. H. Hutchinson, T. C. Jernigan, D. S. Gray, M. Groth, D. A. Humphreys, C. J. Lasnier, R. A. Moyer, P. B. Parks, M. L. Reinke, D. L. Rudakov, E. J. Strait, J. L. Terry, J. Wesley, W. P. West, G. Wurden, and J. Yu, Nucl. Fusion **47**, 1086 (2007).
[7]G. Pautasso, C. J. Fuchs, O. Gruber, C. F. Maggi, M. Maraschek, T. Pütterich, V. Rohde, C. Wittmann, E. Wolfrum, P. Cierpka, M. Beck, and the ASDEX Upgrade Team, Nucl. Fusion **47**, 900 (2007).
[8]E. M. Hollmann, T. C. Jernigan, M. Groth, D. G. Whyte, D. S. Gray, M. E. Austin, B. D. Bray, D. P. Brennan, N. H. Brooks, T. E. Evans, D. A. Humphreys, C. J. Lasnier, R. A. Moyer, A. G. McLean, P. B. Parks, V. Rozhansky, D. L. Rudakov, E. J. Strait, and W. P. West, Nucl. Fusion **45**, 1046 (2005).
[9]Yu. A. Sokolov, JETP Lett. **29**, 244 (1979).
[10]R. Jaspers, K. H. Finken, G. Mank, F. Hoenen, J. A. Boedo, N. J. L. Cardozo, and F. C. Schuller, Nucl. Fusion **33**, 1775 (1993).
[11]R. D. Gill, B. Alper, M. de Baar, T. C. Hender, M. F. Johnson, V. Riccardo, and the EFDA-JET Team, Nucl. Fusion **42**, 1039 (2002).
[12]S. A. Bozhenkov, M. Lehnen, K. H. Finken, M. W. Jakubowski, R. C. Wolf, R. Jaspers, M. Kantor, O. V. Marchuk, E. Uzgel, G. van Wassenhove, O. Zimmerman, D. Reiter, and the TEXTOR Team, Plasma Phys. Controlled Fusion **50**, 105007 (2008).
[13]H. Tamai, R. Yoshino, S. Tokuda, G. Kurita, Y. Neyatani, M. Bakhtiari, R. R. Khayrutdinov, V. E. Lukash, M. N. Rosenbluth, and the JT-60 Team, Nucl. Fusion **42**, 290 (2002).
[14]D. G. Whyte, R. Granetz, V. Izzo, M. Reinke, G. Olynyk, and the Alcator C-Mod Team, **54**, 219 (2009).
[15]R. Jaspers, N. J. Lopes Cardozo, A. J. H. Donne, H. L. M. Widdershoven, and K. H. Finken, Rev. Sci. Instrum. **72**, 466 (2001).
[16]P. Gendrih, A. Grosman, and H. Capes, Plasma Phys. Controlled Fusion **38**, 1653 (1996).
[17]R. Yoshino and S. Tokuda, Nucl. Fusion **40**, 1293 (2000).
[18]M. Lehnen, S. A. Bozhenkov, and S. S. Abdullaev (TEXTOR Team), and M. W. Jakubowski, Phys. Rev. Lett. **100**, 255003 (2008).
[19]J. L. Luxon, Nucl. Fusion **42**, 614 (2002).
[20]M. N. Rosenbluth and S. V. Putvinski, Nucl. Fusion **37**, 1355 (1997).
[21]V. A. Izzo, E. M. Hollmann, A. N. James, D. G. Whyte, G. Olynyk, and L. Lao, Bull. Am. Phys. Soc. **51**, 59 (2009).
[22]E. M. Hollmann, T. C. Jernigan, P. B. Parks, J. A. Boedo, T. E. Evans, M. Groth, D. A. Humphreys, A. N. James, M. J. Lanctot, D. Nishijima, D. L. Rudakov, H. A. Scott, E. J. Strait, M. A. Van Zeeland, J. C. Wesley, W. P. West, W. Wu, and J. H. Yu, Nucl. Fusion **48**, 115007 (2008).
[23]L. R. Baylor, S. K. Combs, C. R. Foust, T. C. Jernigan, S. J. Meitner, P. B. Parks, J. B. Caughman, D. T. Fehling, S. Maruyama, A. L. Qualls, D. A. Rasmussen, and C. E. Thomas, Nucl. Fusion **49**, 085013 (2009).
[24]P. B. Parks, "Dust ball pellets for disruption mitigation," Invention Disclosure DOE Case No. S-113–472 (2007).
[25]T. E. Evans, private communication (2006).
[26]E. M. Hollmann, A. N. James, P. B. Parks, T. E. Evans, D. A. Humphreys, G. L. Jackson, T. C. Jernigan, R. J. La Haye, E. J. Strait, W. P. West, W. Wu, and J. H. Yu, AIP Conf. Proc. **1161**, 65 (2009).
[27]V. Yu. Sergeev, O. A. Bakhareva, B. V. Kuteev, and M. Tendler, Plasma Phys. Rep. **32**, 363 (2006).
[28]P. B. Parks and M. N. Rosenbluth, Phys. Plasmas **5**, 1380 (1998).
[29]R. Yoshino, T. Kondoy, Y. Neyatani, K. Itami, Y. Kawano, and N. Isei, Plasma Phys. Controlled Fusion **39**, 3113 (1997).
[30]P. Helander, L. G. Eriksson, and F. Andersson, Phys. Plasmas **7**, 4106 (2000).
[31]R. W. Harvey, V. S. Chan, S. C. Chiu, T. E. Evans, M. N. Rosenbluth, and D. G. Whyte, Phys. Plasmas **7**, 4590 (2000).
[32]H. Dreicer, Phys. Rev. **115**, 238 (1959).
[33]H. M. Smith and E. Verwichte, Phys. Plasmas **15**, 072502 (2008).
[34]P. V. Savrukhin, Plasma Phys. Controlled Fusion **48**, B201 (2006).